RSC Advances

PAPER

View Article Online
View Journal | View Issue

Cite this: *RSC Adv.*, 2021, **11**, 12107

High chlorine evolution performance of electrochemically reduced TiO_2 nanotube array coated with a thin RuO_2 layer by the self-synthetic method†

Teayoung Lee,[a] Woonghee Lee,[b] Seongsoo Kim,[a] Changha Lee,[a] Kangwoo Cho,[b] Choonsoo Kim *[c] and Jeyong Yoon *[ad]

Recently, reduced TiO_2 nanotube arrays *via* electrochemical self-doping (r-TiO_2) are emerging as a good alternative to conventional dimensionally stable anodes (DSAs) due to their comparable performance and low-cost. However, compared with conventional DSAs, they suffer from poor stability, low current efficiency, and high energy consumption. Therefore, this study aims to advance the electrochemical performances in the chlorine evolution of r-TiO_2 with a thin RuO_2 layer coating on the nanotube structure (RuO_2@r-TiO_2). The RuO_2 thin layer was successfully coated on the surface of r-TiO_2. This was accomplished with a self-synthesized layer of ruthenium precursor originating from a spontaneous redox reaction between Ti^{3+} and metal ions on the r-TiO_2 surface and thermal treatment. The thickness of the thin RuO_2 layer was approximately 30 nm on the nanotube surface of RuO_2@r-TiO_2 without severe pore blocking. In chlorine production, RuO_2@r-TiO_2 exhibited higher current efficiency (~81.0%) and lower energy consumption (~3.0 W h g^{-1}) than the r-TiO_2 (current efficiency of ~64.7% of and energy consumption of ~5.2 W h g^{-1}). In addition, the stability (*ca.* 22 h) was around 20-fold enhancement in RuO_2@r-TiO_2 compared with r-TiO_2 (*ca.* 1.2 h). The results suggest a new route to provide a thin layer coating on r-TiO_2 and to synthesize a high performance oxidant-generating anode.

Received 12th November 2020
Accepted 15th February 2021

DOI: 10.1039/d0ra09623g

rsc.li/rsc-advances

1. Introduction

The electrochemical oxidation process (EOP) has emerged as an alternative to the conventional oxidation process because of its relatively simple facilities, maintenance, and accessibility.[1–8] In addition, as the need for a decentralized water treatment system has increased, the spectrum of EOP's application is broadening from urban to rural areas and developing countries.[2,4,9–11] The process controls contaminants by generating oxidants on-site. In particular, chlorine (Cl_2) has been widely used to remove microorganisms, organic matters, and ammonia effectively along with other oxidants such as ozone, hydroxyl, and sulphate radicals.[1,4,5,10,12–16] The generated Cl_2 diffuses to the bulk solution (below eqn (1)–(3)), and they exist three major species including Cl_2 (pH < 3), HOCl (pH 3–8), and OCl^- (pH > 8).[1]

$$2Cl^- \rightarrow Cl_{2(aq)} + 2e^- \ (E^0 = 1.36 \text{ V } \textit{vs.} \text{ NHE}) \quad (1)$$

$$Cl_{2(aq)} + H_2O \rightarrow HOCl + Cl^- + H^+ \quad (2)$$

$$HOCl \leftrightarrow OCl^- + H^+ \quad (3)$$

Moreover, Cl_2 is considered as a disinfectant to protect from the infectious COVID-19 in the water, sanitation, and hygiene (WASH) field by World Health Organization (WHO),[17] and several researchers suggested using it for treating the wastewater from hospital or household against potentially dangerous coronavirus.[18,19] Thus, practically, the Cl_2 generation system by EOP has a lot of attention with the advantages and is thought to be a suitable technology for small communities to overcome the disease.

For the high efficiency of EOP, the anode material is a pivotal factor governing oxidant species, energy consumption, and cost-effectiveness. A dimensionally stable anode (DSA; RuO_2, IrO_2, *etc.*) has an excellent electrochemical property for chlorine evolution reaction (ClER),[5,14,20–27] but, one obstacle in the effective use of DSA is the high manufacturing cost based on the inclusion of expensive noble metals.

[a]*School of Chemical and Biological Engineering, Institute of Chemical Processes (ICP), Seoul National University, 1 Gwanak-ro, Gwanak-gu, Seoul 08826, Republic of Korea. E-mail: jeyong@snu.ac.kr*

[b]*Division of Environmental Science & Engineering, POSTECH, 77 Chungam-ro, Nam-gu, Pohang 37673, Republic of Korea*

[c]*Department of Environmental Engineering, Institute of Energy/Environment Convergence Technologies, Kongju National University, 1223-24, Cheonan-daero, Cheonan-si 31080, Republic of Korea. E-mail: choonsoo@kongju.ac.kr*

[d]*Korea Environment Institute, 370 Sicheong-daero, Sejong-si 30147, Republic of Korea*

† Electronic supplementary information (ESI) available. See DOI: 10.1039/d0ra09623g

In this regard, recently, a reduced TiO_2 nanotube array (r-TiO_2), which can be simply fabricated by electrochemical self-doping of an anatase TiO_2 nanotube array (a-TiO_2), has attracted much attentions as a promising electrode in electrochemical ClER.[11,28–30] The self-doping simply converts Ti^{4+} in a-TiO_2 to Ti^{3+} *via* the intercalation of protons as self-dopants, potentially leading to high electrocatalytic activity in the generation of oxidants with high surface area and low-cost.[28,31] In spite of its advantages, r-TiO_2 has unfortunately suffered from a poor long-term service time, low current efficiency and high energy consumption in chlorine production.

Therefore, this study aimed to enhance the chlorine generation performance of r-TiO_2 with a simple thin layer coating of RuO_2 as an excellent anode material (RuO_2@r-TiO_2). This RuO_2 thin layer was coated on the surface of r-TiO_2 *via* the spontaneous reduction of ruthenium precursor resulting from a partial conversion reaction of Ti^{3+} to Ti^{4+} (ref. 32 and 33) in r-TiO_2 and the followed thermal treatment, successfully leading to the improvement of electrocatalyst for chlorine evolution. To fully understand its surface properties, we used field emission scanning electron microscopy (FE-SEM), field emission transmission electron microscopy (FE-TEM), X-ray diffraction (XRD) and X-ray photoelectron spectroscopy (XPS). The electrocatalytic activity for ClER was investigated with cyclic voltammetry (CV) measurement and the *N*,*N*-diethyl-*p*-phenylenediamine (DPD) method. Furthermore, scanning electrochemical microscopy (SECM) was employed as an *in situ* analysis to investigate the enhanced ClER from the uniformly coated RuO_2 on the r-TiO_2.

2. Materials and methods

2.1 Preparation of r-TiO_2 and RuO_2@TiO_2

r-TiO_2 was prepared by a typical two-step anodization method and electrochemical self-doping. First, the Ti foil was anodized at 60 V for 2 h in an ethylene-glycol-based electrolyte containing DI water (2.5 wt%) and NH_4F (0.2 wt%). The formed nanotube film was peeled off by a compressed air stream, and then a second-anodization was conducted at 40 V for 7 h under the same electrolyte condition. By annealing the as-prepared TiO_2 NTA at 450 °C for 1 h in air, the crystal structure was converted into an anatase-dominant phase (a-TiO_2).[34] Then, electrochemical doping was performed on the a-TiO_2 under cathodic polarization with constant current (16.7 mA cm^{-2}) for 90 s in a phosphate buffer solution ($[KH_2PO_4]_0$ = 0.1 M with KOH, pH = 7.02).[28–30] The prepared r-TiO_2 had a thickness of approximately 13.8 μm and the width of the nanotubes was 130 ± 30 nm (Fig. S1†).

Prior to the RuO_2 coating process, the r-TiO_2 was fully dried at room temperature, then immersed in an aqueous ruthenium precursor solution (5 mM $RuCl_3 \cdot H_2O$ in deionized (DI) water) under the dark condition for 24 h to produce the self-synthesized coating (Ru@r-TiO_2). After that, the treated r-TiO_2 was fully washed with DI water to remove the remained ruthenium precursor in the nanotubes, then annealed in 450 °C (air) for 1 h to be oxidized (RuO_2@r-TiO_2). The process is presented briefly in Fig. 1.

2.2 Characterization of RuO_2@r-TiO_2

The morphologies of r-TiO_2 and RuO_2@r-TiO_2 were observed with field emission scanning electron microscopy (FE-SEM, JSM-6701F, JEOL, Japan) at 20 kV, and field emission transmission electron microscopy (FE-TEM, JEM-F200, JEOL, Japan) was employed to confirm the deposited RuO_2 layer on the wall of r-TiO_2 including energy-dispersive X-ray spectroscopy (EDS). An X-ray diffractometer (XRD, Bruker D8 DISCOVER, Germany) and X-ray photoelectron spectroscope (XPS, Sigma Probe, ThermoVG, UK) were used to examine the material species of the TiO_2 NTA-based electrodes.

2.3 Evaluation of electrochemical properties of RuO_2@TiO_2

The electrochemical properties of RuO_2@r-TiO_2 were investigated by cyclic voltammetry (CV) measurement with a three-electrodes system (reference electrode: Ag/AgCl in sat. KCl, counter electrode: Pt mesh) at a scan rate of 5 mV s^{-1}. To understand the electrocatalytic activity of RuO_2@r-TiO_2, chlorine was electrochemically produced in a two-electrodes system that consisted of RuO_2@r-TiO_2 as an anode and Pt mesh as a cathode with a constant current density of 16.7 mA cm^{-2} in 0.1 M NaCl. The produced chlorine concentration was monitored by the *N*,*N*-diethyl-*p*-phenylenediamine (DPD) method with a spectrophotometer (DR 900, Hach Co., USA, 530 nm). The current efficiency (%) and the energy consumption (W h g^{-1}) of chlorine generation were calculated by eqn (4) and (5).

$$\text{Current efficiency } (\%) = \frac{c \times V \times n \times F}{M(Cl_2) \times I \times t} \times 100 \quad (4)$$

$$\text{Energy consumption } (\text{W h g}^{-1}) = \frac{I \times \int e\mathrm{d}t}{c \times V} \quad (5)$$

where c is the concentration of generated chlorine (g L^{-1}), V is the electrolyte volume (L), n is the electrons' number (1 eq. mol^{-1}), F is the faradaic constant (96 485 C $eq.^{-1}$), $M(Cl_2)$ is the molecular

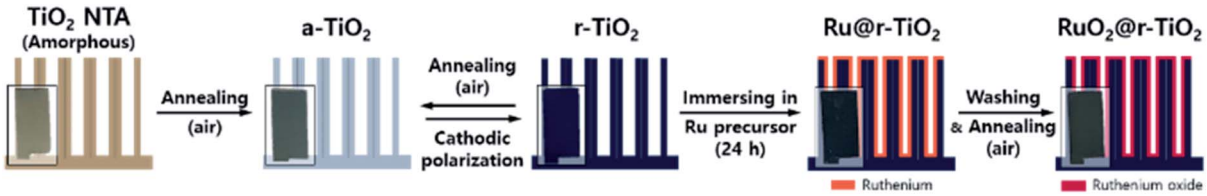

Fig. 1 Scheme of thin RuO_2 layer coating process on reduced TiO_2 nanotube array *via* electrochemical self-doping.

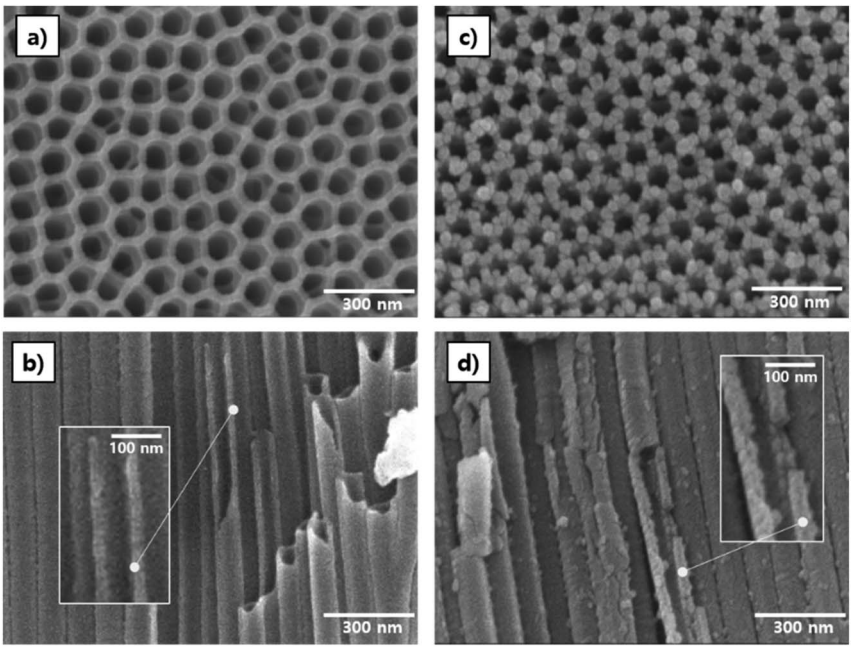

Fig. 2 Morphologies of (a) top- (b) cross sectional view of r-TiO_2 and (c) top- (d) cross sectional view of RuO_2 @r-TiO_2 with a field emission scanning electron microscope (FE-SEM).

weight of chlorine (71 g mol^{-1}), I is the applied constant current (C s^{-1}), t is the operation time (s), and e is the cell voltage (V).

To confirm the chlorine evolution mechanism of RuO_2@r-TiO_2, the hydroxyl radical production was investigated with a degradation of terephthalic acid (TA) as a probe compound. In addition, the effect of hydroxyl radical on chlorine evolution was examined by adding 1 M *t*-BuOH. The TA degradation was measured by high-performance liquid chromatography (HPLC; Ultimate 3000, Dionex, Sunnyvale, CA, USA) in the methanol and formic acid (0.1%) mixture eluent (v/v, 60 : 40).[35] Furthermore, scanning electrochemical microscopy [SECM; SP-300 (bipotentiostat), M470 (SECM Workstation, Bio-Logics SAS), France] was performed to scrutinize the activities for ClER on samples as an *in situ* measurement. This visualized the scanned area (500 μm × 500 μm of the electrodes) with a colour gradation from blue to red.

3. Results and discussion

3.1 Morphology of RuO_2@r-TiO_2

Fig. 2 shows FE-SEM images (top and cross sectional view) of r-TiO_2 and RuO_2@r-TiO_2. As can be seen in Fig. 2, significant differences on the nanotube edge and sidewall of RuO_2@r-TiO_2 were found. The RuO_2@r-TiO_2 revealed that a large number of nano-grains were formed on the verges of the nanopore entrances compared to the r-TiO_2 in Fig. 2a and c. In addition, the sidewall of RuO_2@r-TiO_2 was thicker after deposition on r-

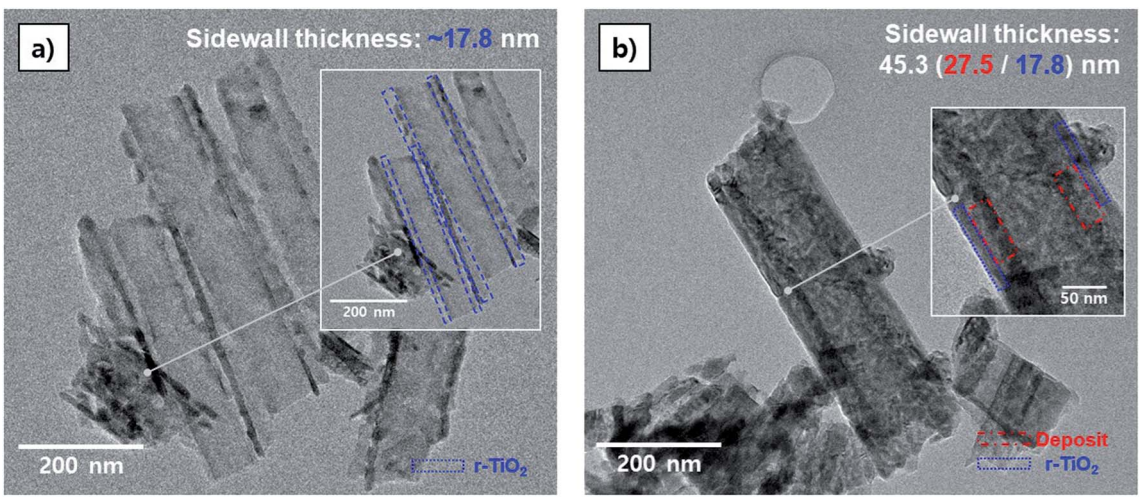

Fig. 3 Nanotube structure characterization of (a) r-TiO_2 and (b) RuO_2@r-TiO_2 using field emission transmission electron microscope (FE-TEM).

TiO_2 (Fig. 2b and d). It seems that the assembles of nano-grains on the sidewall of the inner pore were formed to a thin layer (see inset image of Fig. 2d).

The sidewall condition of RuO_2@r-TiO_2 is inspected meticulously by FE-TEM in Fig. 3. Considering the thickness of the r-TiO_2 sidewall (*ca.* 14–22 nm), the sidewall thickness of RuO_2@r-TiO_2 (*ca.* ~45.3 nm) was approximately three times thicker. With the distinguished interface layer at RuO_2@r-TiO_2 (red dashed square in inset image of Fig. 3b) and the results of EDS in Fig. S2,† we see that RuO_2 was successfully deposited on the sidewall of RuO_2@r-TiO_2. It is plausible that the RuO_2@r-TiO_2 revealed a fine coating on the overall surface of r-TiO_2 with open-top and hollow nanotube structure *via* the self-synthesized coating method.

3.2 Characteristics of the deposits on RuO_2@r-TiO_2

To better understand the deposits on RuO_2@r-TiO_2, the XRD patterns and XPS spectra of as-prepared r-TiO_2 and RuO_2@r-TiO_2 are further analysed in Fig. 4. From the results of the XRD patterns in Fig. 4a, an elusive peak appears at 28° with regard to RuO_2 at RuO_2@r-TiO_2.[36–38] Hence, the coated RuO_2 is examined in detail through the XPS results of Ru 3d, O 1s, and Ti 2p in Fig. 4b–d. As shown in Fig. 4b, the RuO_2@r-TiO_2 exhibited a clear RuO_2 peak at 280.4 eV in the XPS spectra of Ru $3d_{5/2}$.[38–43] From the shoulder peak (529.4 eV) in XPS spectra of O 1s (red line in Fig. 4c), the deposition of RuO_2 was further confirmed.[38,39,44–46] Moreover, this is clearly supported by the peak shift (1.2 eV) from 458.9 to 457.7 eV in Fig. 4d of Ti $2p_{3/2}$ indicating a heterojunction of RuO_2 and TiO_2.[40,42,47]

These results suggest that the RuO_2 thin layer was well-formed on the overall surface of RuO_2@r-TiO_2 *via* the self-synthesized coating method. Note that the self-synthesis method has been reported in the nanoparticles of noble metals on a TiO_2 sphere with the spontaneous redox reaction between metal ions and the reduced TiO_2.[32,33] To the best of our knowledge, this is the first report to prepare a thin RuO_2 layer coating on electrochemically reduced TiO_2 NTA *via* the previous phenomenon including the following thermal treatment, without severe pore blockage and toxic chemicals when compared to other methods for treating active materials on the TiO_2 NTAs.[37,48–53]

3.3 Electrocatalytic activities of RuO_2@r-TiO_2

Fig. 5 shows the improved electrochemical properties of RuO_2@r-TiO_2. From the result in Fig. 5a, where the RuO_2@r-TIO_2 initiated an oxygen evolution reaction (OER) at a potential of approximately 1.1 V *vs.* Ag/AgCl, the over-potential of which decreased significantly by up to 1.0 V compared to the r-TiO_2. This means that the surface of RuO_2@r-TiO_2 had a higher electrocatalytic activity for OER when assisted by the thin RuO_2 layer. In the cathodic biased potential regime ranging from 0 to −1.5 V *vs.* Ag/AgCl on the RuO_2@r-TiO_2, there were no reactions regarding proton inter/deintercalation (−0.6/−0.9 V *vs.* Ag/AgCl) which was obviously found on r-TiO_2 (blue dash line in the inset image of Fig. 5a) as a unique electrochemical feature of r-TiO_2.[28,54–57] Additionally, as shown in Fig. S3,† in contrast to RuO_2@r-TiO_2, the r-TiO_2 lost its electrochemical property after the thermal treatment. This implies that the self-synthesized coating covered the entire surface of the r-TiO_2 and that the r-TiO_2 under the deposit of RuO_2@r-TiO_2 was prevented from oxidizing during the thermal treatment. Accordingly, its electrochemical property did not vanish even when it was annealed in the air condition; rather, this property was improved by the formed RuO_2.

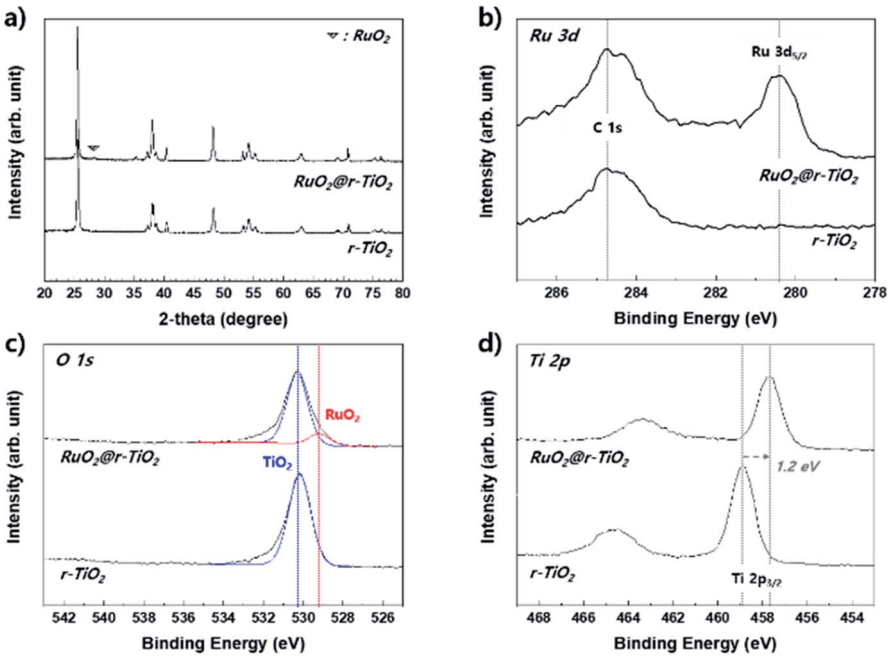

Fig. 4 (a) XRD patterns and XPS spectra (b) Ru 3d, (c) O 1s, and (d) Ti 2p of r-TiO_2 and RuO_2@r-TiO_2.

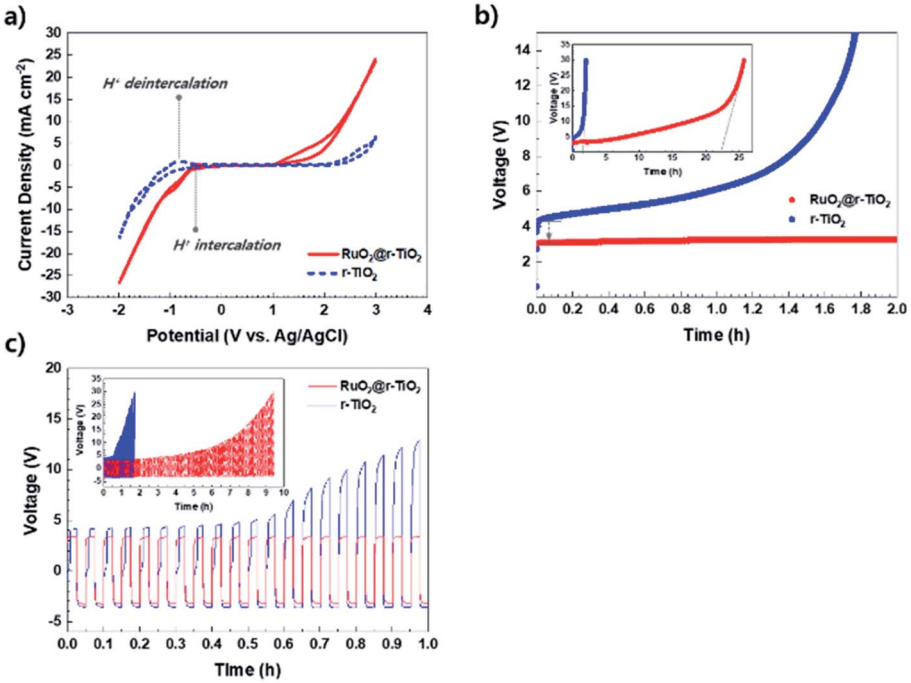

Fig. 5 (a) Cyclic voltammograms (CV) (scan rate: 5 mV s^{-1}), the stability test with (b) applied constant current density (16.7 mA cm^{-2}), and (c) polarity reversal operation (±16.7 mA cm^{-2}, switching time 90 s) of r-TiO$_2$ and RuO$_2$@r-TiO$_2$ in 0.1 M phosphate buffer solution (PBS).

For oxygen evolution under a constant current condition (Fig. 5b), RuO$_2$@r-TiO$_2$ led to a lower initial operational cell voltage (~3.0 V) than r-TiO$_2$ (~4.2 V), and it showed significantly enhanced stability with a value that was approximately 20 times higher (~22 h) than that of r-TiO$_2$ (~1.2 h). This can be evaluated based on the drastic increase in cell voltage. In addition, under a polarity reversal operation (switching constant current for +16.7 mA cm^{-2} *vs.* −16.7 mA cm^{-2}), the RuO$_2$@r-TiO$_2$ was highly stable on the stress from the harsh reversal condition compared to r-TiO$_2$. This indicates that RuO$_2$@r-TiO$_2$ is a more reliable material than r-TiO$_2$ in various environmental and industrial applications. Nevertheless, for the further success of

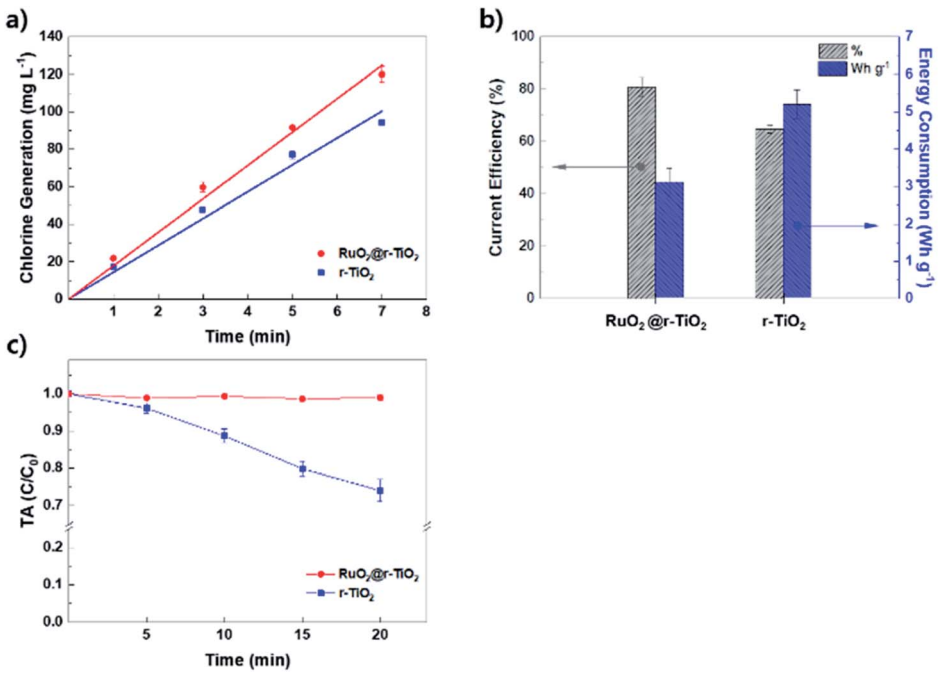

Fig. 6 (a) Evolution of chlorine (16.7 mA cm^{-2}, 0.1 M NaCl) and (b) the current efficiency and energy consumption in 3 min, and (c) terephthalic acid (TA) degradation for hydroxyl radical measurement (0.1 mM TA, 16.7 mA cm^{-2}) of RuO$_2$@r-TiO$_2$ and r-TiO$_2$.

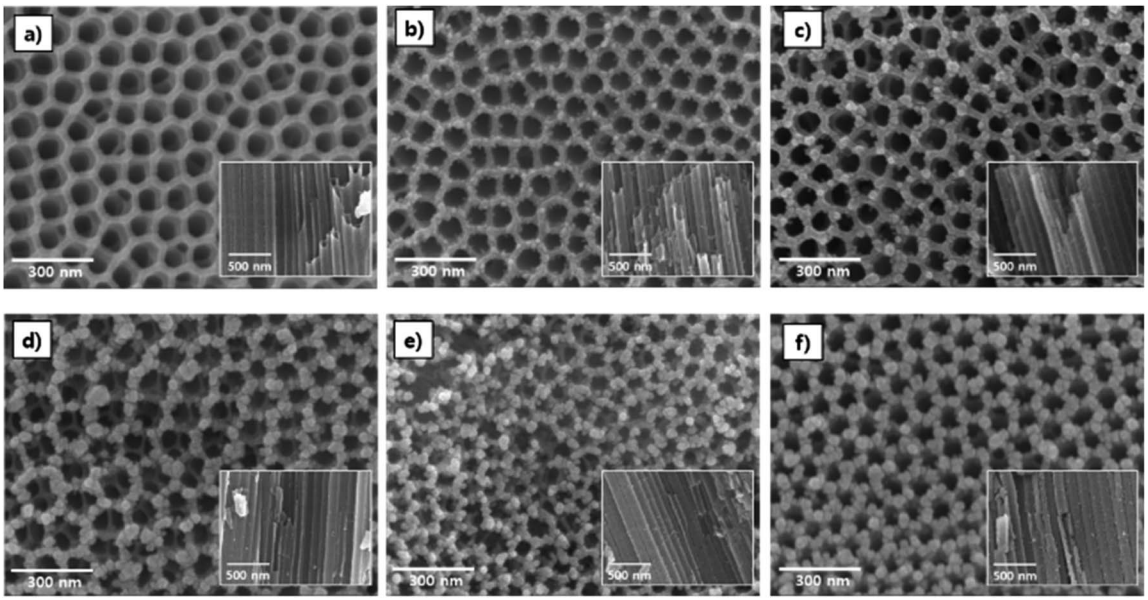

Fig. 7 FE-SEM images (cross sectional view in inset images) of (a) r-TiO_2 and RuO_2 coated electrodes after immersion in 5 mM aqueous ruthenium precursor for (b) 1, (c) 3, (d) 6, (e) 12, and (f) 24 h. Note that FE-SEM images of r-TiO_2 and RuO_2@r-TiO_2 (24 h) were from the result of Fig. 2 in order to compare the morphologies of each electrode.

RuO_2@r-TiO_2, the long-term performance stability must be improved *via* controlling the doping level of r-TiO_2 (Fig. S4 in ESI†). It is required to further study the effect of type of catalyst (*i.e.*, IrO_2, Pt and carbon, *etc.*) for thin layer coating, coating thickness, and temperature of thermal treatment on CIER.

Fig. 6 shows the enhanced chlorine evolution performance and the pathway for ClER of RuO_2@r-TiO_2 compared to r-TiO_2. As shown in Fig. 6a, the chlorine production rate of RuO_2@r-TiO_2 was estimated to be approximately 17.85 mg L^{-1} min^{-1}. This is approximately 20% faster than that of r-TiO_2 (14.35 mg L^{-1} min^{-1}). Correspondingly, RuO_2@r-TiO_2 exhibited a current efficiency of 81.0% with an energy consumption of 3.0 W h g^{-1}, indicating higher electrocatalytic activity for chlorine production compared to r-TiO_2 (current efficiency of 64.7% and energy consumption of 5.2 W h g^{-1} in Fig. 6b). The high chlorine evolution performances can be explained by the uniformly organized nanotube structure with the thin RuO_2 layer.

Furthermore, with the thin RuO_2 layer, the surface of RuO_2@r-TiO_2 was converted to be more attractive for chlorine than hydroxyl radical (Fig. 6c). This resulted in excellent chlorine production performances, namely the RuO_2@r-TiO_2 can be defined as an active electrode (high efficiency for chlorine production; RuO_2, IrO_2, *etc.*) rather than an inactive electrode (high efficiency for hydroxyl radical; r-TiO_2, boron doped diamond electrode, SnO_2, PbO_2, *etc.*).[5,14,20,28,37] Note that, in common, the active electrode produces CIER *via* direct electron transfer with chloride ions whereas the inactive electrode leads to CIER by the indirect pathway mediated by hydroxyl radicals.

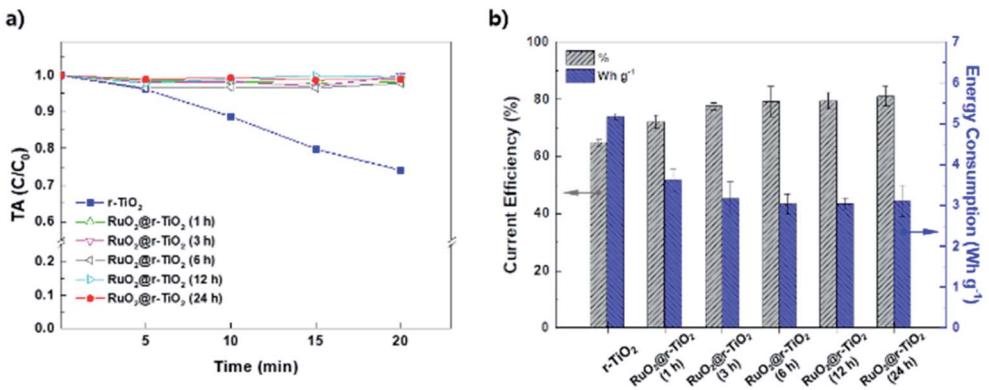

Fig. 8 (a) OH radical generation measurement with TA degradation (0.1 mM TA, 16.7 mA cm^{-2}) and (b) chlorine generation efficiency and energy consumption (16.7 mA cm^{-2}, 0.1 M NaCl, 3 min) of r-TiO_2 and RuO_2 coated electrodes after immersion in 5 mM aqueous ruthenium precursor for 1, 3, 6, 12, and 24 h. Note that chlorine generation efficiency, energy consumption, and the TA degradation data of r-TiO_2, and RuO_2@r-TiO_2 (24 h) are from the results of Fig. 6.

This is well supported by the effect of the hydroxyl radical scavenger on the chlorine evolution (Fig. S5†). With the addition of *t*-BuOH as hydroxyl radical scavenger, the chlorine evolution efficiency of RuO_2@r-TiO_2 did not meaningfully decrease, whereas that of r-TiO_2 was significantly reduced. This means the small effect of hydroxyl radical on the chlorine evolution of RuO_2@r-TiO_2 instead of r-TiO_2 produced chlorine mediated by hydroxyl radical.[39] Considering the effect of hydroxyl radical on CIER of RuO_2@r-TiO_2 and r-TiO_2, the surface of RuO_2@r-TiO_2 behaves active electrodes. Eventually, we see the surface of RuO_2@r-TiO_2 was converted to an active electrode from an inactive electrode. It is attributed to that the RuO_2 thin layer was uniformly coated on the surface of nano-pores of r-TiO_2, and thus, the surface of r-TiO_2 only worked as substrate, not catalytic material.

3.4 Effect of the immersion time on chlorine production efficiency of RuO_2@r-TiO_2

To optimize the deposition of RuO_2 on RuO_2@r-TiO_2, we further investigate the effect of the RuO_2 loading amount controlled *via* Ru precursor dipping time (ranging from 1 to 24 h) on the deposition and chlorine evolution efficiency of RuO_2@r-TiO_2. Fig. 7 shows the morphologies of the RuO_2@r-TiO_2 samples prepared with the time of 1, 3, 6, 12, and 24 h. As shown in Fig. 7, as the immersion time increased, the size of the nano-grains on the nano-pore edge and the thickness of the side-wall (inset images) gradually increased. In particular, regardless of the time, surfaces of all samples were more attractive for chlorine evolution than hydroxyl radical (Fig. 8a). However, compared to the chlorine evolution performances of RuO_2@r-TiO_2 prepared with the immersion times of 6, 12 and 24 h (current efficiency of 79.2, 79.4, and 81.0%; and energy consumption of 3.0, 3.0, 3.0 W h g^{-1}, respectively), the RuO_2@r-TiO_2 prepared with immersion times of 1 and 3 h resulted in relatively low chlorine evolution performance with current efficiencies of 72.2, 77.6% and energy consumption of 3.6, 3.2 W h g^{-1}, respectively (see Fig. 8b, and refer to all data of chlorine generation in Fig. S6a†). Correspondingly, a similar trend in the long-term stability was found (Fig. S6b†).

Moreover, this is well supported by the results obtained with the sample generation/tip collection (SG/TC) mode of SECM (Fig. 9) which visualized the electrocatalytic activity for chlorine production *via* a chlorine reduction reaction at −0.2 V *vs.* Ag/AgCl (the detailed experimental condition are shown in Fig. S7 and S8†).[58,59] As shown in Fig. 9, the electrocatalytic activity was evenly enhanced across the entire surface after 12 h according to the condition of deposited RuO_2 confirmed previously in Fig. 7 with FE-SEM. Particularly, compared to the pristine r-TiO_2 (Fig. 9a) which revealed nano-patterns of

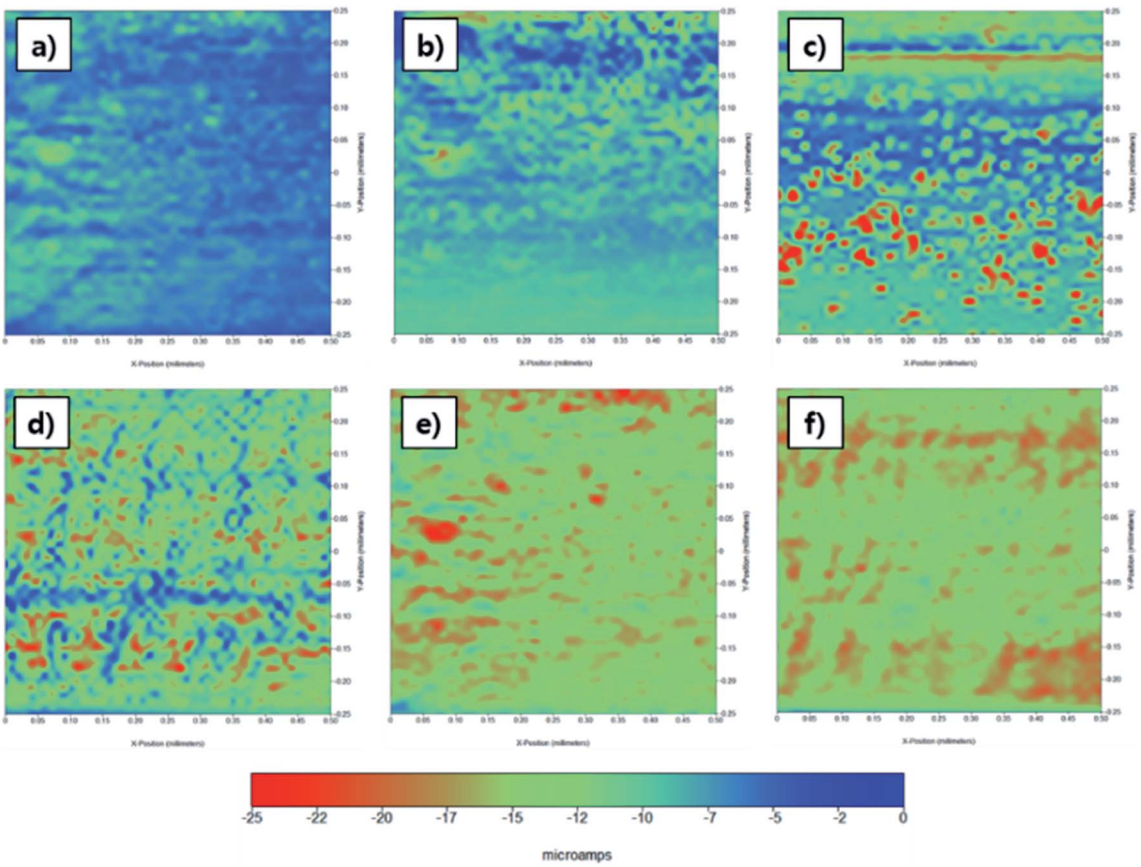

Fig. 9 Area scan of scanning electrochemical microscopy (SECM) in 0.1 M NaCl, 16.7 mA cm^{-2}; (a) r-TiO_2, RuO_2 coated electrodes after immersing in 5 mM aqueous ruthenium precursor for (b) 1, (c) 3, (d) 6, (e) 12, and (f) 24 h.

emerald-colored rings, reddish cores were observed after commencing RuO_2 deposition on r-TiO_2 (Fig. 9b–f). The RuO_2 coated inner pores improved the chlorine generation inside of the nanotubes, so that the higher activity (red) was measured at the center of the patterns than the circular edge. In Fig. 9f, circular nano-patterns on RuO_2@r-TiO_2 (24 h) were uniformly distributed in red. This color change verifies that the RuO_2 was effectively coated at the top edge of the tubes and even at its inner-pores as previously shown in images of SEM and TEM (Fig. 2 and 3), resulting in the enhanced the electrocatalytic performance for the CIER. As such, the morphological and electrochemical properties of r-TiO_2 are feasible to be facilely controlled with the self-synthesis coating method that can be extended to various fields of studies utilizing TiO_2 NTA-based electrocatalysts.

4. Conclusions

In this study, we successfully fabricated the RuO_2@r-TiO_2 with a self-synthesized coating method leading to a RuO_2 thin layer coating on r-TiO_2 and demonstrated considerably enhanced electro-catalytic activity for chlorine production. The fine RuO_2 coating was achieved *via* the self-synthesized coating originating from the conversion of Ti^{3+} to Ti^{4+} on r-TiO_2 and thermal treatment under the atmospheric condition. Using various surface analysis including FE-SEM, FE-TEM, EDS and XPS, the formation of a RuO_2 thin layer (thickness of ~27.5 nm) on the inner pore sidewall of RuO_2@r-TiO_2 was clearly proven. The RuO_2@r-TiO_2 exhibited the highly enhanced electrocatalytic activity for chlorine production with the production rate of 17.85 mg L^{-1} min^{-1}, the high current efficiency of 81.0%, energy consumption of 3.0 W h g^{-1}, and long-term stability of ~22 h compared to r-TiO_2 (production rate of 14.35 mg L^{-1} min^{-1}, the current efficiency of 64.7%, energy consumption of 5.2 W h g^{-1}, and long term service time of 1.2 h). In addition, the performances of RuO_2@r-TiO_2 was optimized by controlling the immersion time in the precursor. These results provide a new approach to the thin metal oxide coating on r-TiO_2 and provide opportunities for various applications such as electrolysis, photo-catalyst, and energy storage devices.

Conflicts of interest

There are no conflicts to declare.

Acknowledgements

This research was supported by the Technology Innovation Program (10082572, Development of Low Energy Desalination Water Treatment Engineering Package System for Industrial Recycle Water Production) funded by the Ministry of Trade, Industry & Energy (MOTIE, Korea) and the National Research Foundation of Korea (NRF) grant funded by the Ministry of Science and ICT of the Korea Government (MSIT) (NRF-2019R1G1A1003336).

References

1 Z. Chen, Y. Liu, W. Wei and B. Ni, Recent advances in electrocatalysts for halogenated organic pollutant degradation, *Environ. Sci.: Nano*, 2019, **6**, 2332.
2 S. O. Ganiyu, C. A. Martínez-Huitle and M. A. Rodrigo, Renewable energies driven electrochemical wastewater/soil decontamination technologies: a critical review of fundamental concepts and applications, *Appl. Catal., B*, 2020, **270**, 118857.
3 V. Poza-Nogueiras, M. Pazos, M. Á. Sanromán and E. González-Romero, Double benefit of electrochemical techniques: treatment and electroanalysis for remediation of water polluted with organic compounds, *Electrochim. Acta*, 2019, **320**, 1–13.
4 B. C. Hodges, E. L. Cates and J. H. Kim, Challenges and prospects of advanced oxidation water treatment processes using catalytic nanomaterials, *Nat. Nanotechnol.*, 2018, **13**, 642–650.
5 M. Panizza and G. Cerisola, Direct and Mediated Anodic Oxidation of Organic Pollutants, *Chem. Rev.*, 2009, **109**, 6541–6569.
6 F. C. Moreira, R. A. R. Boaventura, E. Brillas and V. J. P. Vilar, Electrochemical advanced oxidation processes: a review on their application to synthetic and real wastewaters, *Appl. Catal., B*, 2017, **202**, 217–261.
7 C. A. Martínez-Huitle and S. Ferro, Electrochemical oxidation of organic pollutants for the wastewater treatment: direct and indirect processes, *Chem. Soc. Rev.*, 2006, **35**, 1324–1340.
8 J. Grimm, D. Bessarabov and R. Sanderson, Review of electro-assisted methods for water purification, *Desalination*, 1998, **115**, 285–294.
9 K. Cho and M. R. Hoffmann, Urea degradation by electrochemically generated reactive chlorine species: products and reaction pathways, *Environ. Sci. Technol.*, 2014, **48**, 11504–11511.
10 X. Huang, Y. Qu, C. A. Cid, C. Finke, M. R. Hoffmann, K. Lim and S. C. Jiang, Electrochemical disinfection of toilet wastewater using wastewater electrolysis cell, *Water Res.*, 2016, **92**, 164–172.
11 Y. Yang and M. R. Hoffmann, Synthesis and Stabilization of Blue-Black TiO_2 Nanotube Arrays for Electrochemical Oxidant Generation and Wastewater Treatment, *Environ. Sci. Technol.*, 2016, **50**, 11888–11894.
12 S. Trasatti, Electrochemistry and environment: the role of electrocatalysis, *Int. J. Hydrogen Energy*, 1995, **20**, 835–844.
13 H. F. Diao, X. Y. Li, J. D. Gu, H. C. Shi and Z. M. Xie, Electron microscopic investigation of the bactericidal action of electrochemical disinfection in comparison with chlorination, ozonation and Fenton reaction, *Process Biochem.*, 2004, **39**, 1421–1426.
14 C. Comninellis, Electrocatalysis in the Electrochemical Conversion/Combustion of Organic Pollutants for Waste Water Treatment, *Electrochim. Acta*, 1994, **39**, 1857–1862.

15 J. Kim, C. Lee and J. Yoon, Electrochemical Peroxodisulfate (PDS) Generation on a Self-Doped TiO_2 Nanotube Array Electrode, *Ind. Eng. Chem. Res.*, 2018, **57**, 11465–11471.
16 J. Jeong, C. Kim and J. Yoon, The effect of electrode material on the generation of oxidants and microbial inactivation in the electrochemical disinfection processes, *Water Res.*, 2009, **43**, 895–901.
17 *Water, sanitation, hygiene and waste management for SARS-CoV-2, the virus that causes COVID-19*, World Health Organization, https://www.who.int/publications/i/item/WHO-2019-nCoV-IPC-WASH-2020.4, accessed Oct. 2020.
18 G. D. Bhowmick, D. Dhar, D. Nath, M. M. Ghangrekar, R. Banerjee, S. Das and J. Chatterjee, Coronavirus disease 2019 (COVID-19) outbreak: some serious consequences with urban and rural water cycle, *npj Clean Water*, 2020, **3**, 32.
19 J. Wang, J. Shen, D. Ye, X. Yan, Y. Zhang, W. Yang, X. Li, J. Wang, L. Zhang and L. Pan, Disinfection technology of hospital wastes and wastewater: suggestions for disinfection strategy during coronavirus disease 2019 (COVID-19) pandemic in China, *Environ. Pollut.*, 2020, **262**, 114665.
20 S. Trasatti, Progress in the Understanding of the Mechanism of Chlorine Evolution at Oxide Electrodes, *Electrochim. Acta*, 1987, **32**, 369–382.
21 C. Comninellis and G. P. Vercesi, Characterization of DSA-type electrodes: choice of a coating, *J. Appl. Electrochem.*, 1991, **21**, 335–345.
22 C. E. Finke, S. T. Omelchenko, J. T. Jasper, M. F. Lichterman, C. G. Read, N. S. Lewis and M. R. Hoffmann, Enhancing the activity of oxygen-evolution and chlorine-evolution electrocatalysts by atomic layer deposition of TiO_2, *Energy Environ. Sci.*, 2019, **12**, 358–365.
23 Y. Lee, J. Suntivich, K. J. May, E. E. Perry and Y. Shao-Horn, Synthesis and activities of rutile IrO_2 and RuO_2 nanoparticles for oxygen evolution in acid and alkaline solutions, *J. Phys. Chem. Lett.*, 2012, **3**, 399–404.
24 D. Dionisio, L. H. E. Santos, M. A. Rodrigo and A. J. Motheo, Electro-oxidation of methyl paraben on DSA®-Cl_2: UV irradiation, mechanistic aspects and energy consumption, *Electrochim. Acta*, 2020, **338**, 135901.
25 A. Cornell, B. Håkansson and G. Lindbergh, Ruthenium based DSA® in chlorate electrolysis - critical anode potential and reaction kinetics, *Electrochim. Acta*, 2003, **48**, 473–481.
26 K. S. Exner, J. Anton, T. Jacob and H. Over, Controlling selectivity in the chlorine evolution reaction over RuO_2-based catalysts, *Angew. Chem., Int. Ed.*, 2014, **53**, 11032–11035.
27 S. Trasatti, Electrocatalysis: understanding the success of DSA®, *Electrochim. Acta*, 2000, **45**, 2377–2385.
28 C. Kim, S. Kim, J. Choi, J. Lee, J. S. Kang, Y. E. Sung, J. Lee, W. Choi and J. Yoon, Blue TiO_2 nanotube array as an oxidant generating novel anode material fabricated by simple cathodic polarization, *Electrochim. Acta*, 2014, **141**, 113–119.
29 C. Kim, S. Kim, J. Lee, J. Kim and J. Yoon, Capacitive and oxidant generating properties of black-colored TiO_2 nanotube array fabricated by electrochemical self-doping, *ACS Appl. Mater. Interfaces*, 2015, **7**, 7486–7491.
30 C. Kim, S. Kim, S. P. Hong, J. Lee and J. Yoon, Effect of doping level of colored TiO_2 nanotube arrays fabricated by electrochemical self-doping on electrochemical properties, *Phys. Chem. Chem. Phys.*, 2016, **18**, 14370–14375.
31 P. Roy, S. Berger and P. Schmuki, TiO_2 Nanotubes: Synthesis and Applications, *Angew. Chem., Int. Ed.*, 2011, 2904–2939.
32 Z. Zheng, B. Huang, X. Qin, X. Zhang, Y. Dai and M. H. Whangbo, Facile in situ synthesis of visible-light plasmonic photocatalysts M@TiO_2 (M = Au, Pt, Ag) and evaluation of their photocatalytic oxidation of benzene to phenol, *J. Mater. Chem.*, 2011, **21**, 9079–9087.
33 Y. Xie, K. Ding, Z. Liu, R. Tao, Z. Sun, H. Zhang and G. An, In situ controllable loading of ultrafine noble metal particles on titania, *J. Am. Chem. Soc.*, 2009, **131**, 6648–6649.
34 C. Kim, S. Lee, S. Kim and J. Yoon, Effect of Annealing Temperature on the Capacitive and Oxidant-generating Properties of an Electrochemically Reduced TiO_2 Nanotube Array, *Electrochim. Acta*, 2016, **222**, 1578–1584.
35 Y. Jing and B. P. Chaplin, Mechanistic Study of the Validity of Using Hydroxyl Radical Probes to Characterize Electrochemical Advanced Oxidation Processes, *Environ. Sci. Technol.*, 2017, **51**, 2355–2365.
36 M. Etzi Coller Pascuzzi, A. Goryachev, J. P. Hofmann and E. J. M. Hensen, Mn promotion of rutile TiO_2-RuO_2 anodes for water oxidation in acidic media, *Appl. Catal., B*, 2020, **261**, 10.
37 J. Kim, C. Kim, S. Kim and J. Yoon, RuO_2 coated blue TiO_2 nanotube array (blue TNA-RuO_2) as an effective anode material in electrochemical chlorine generation, *J. Ind. Eng. Chem.*, 2018, **66**, 478–483.
38 Q. Gu, Z. Gao, S. Yu and C. Xue, Constructing Ru/TiO_2 Heteronanostructures Toward Enhanced Photocatalytic Water Splitting via a RuO_2/TiO_2 Heterojunction and Ru/TiO_2 Schottky Junction, *Adv. Mater. Interfaces*, 2016, **3**, 17–21.
39 J. F. Moulder, W. F. Stickle, P. E. Sobol and K. D. Bomben, *Handbook of X-ray Photoelectron Spectroscopy*, Physical Electrocnis, Inc., Minesota, 1995.
40 Y. He, D. Langsdorf, L. Li and H. Over, Versatile model system for studying processes ranging from heterogeneous to photocatalysis: epitaxial RuO_2(110) on TiO_2(110), *J. Phys. Chem. C*, 2015, **119**, 2692–2702.
41 D. J. Morgan, Resolving ruthenium: XPS studies of common ruthenium materials, *Surf. Interface Anal.*, 2015, **47**, 1072–1079.
42 M. T. Uddin, Y. Nicolas, C. Olivier, T. Toupance, M. M. Müller, H. J. Kleebe, K. Rachut, J. Ziegler, A. Klein and W. Jaegermann, Preparation of RuO_2/TiO_2 mesoporous heterostructures and rationalization of their enhanced photocatalytic properties by band alignment investigations, *J. Phys. Chem. C*, 2013, **117**, 22098–22110.
43 H. Yue, L. Xue and F. Chen, Efficiently electrochemical removal of nitrite contamination with stable RuO_2-TiO_2/Ti electrodes, *Appl. Catal., B*, 2017, **206**, 683–691.

44 D. D. Sarma and C. N. R. Rao, XPES studies of oxides of second- and third-row transition metals including rare earths, *J. Electron Spectrosc. Relat. Phenom.*, 1980, **20**, 25–45.
45 K. S. Kim and N. Winograd, X-ray Photoelectron Spectroscopic Studies of Ruthenium-Oxygen Surfaces, *J. Catal.*, 1974, **72**, 66–72.
46 J. Y. Shen, A. Adnot and S. Kaliaguine, An ESCA study of the interaction of oxygen with the surface of ruthenium, *Appl. Surf. Sci.*, 1991, **51**, 47–60.
47 W. Ouyang, M. J. Muñoz-Batista, A. Kubacka, R. Luque and M. Fernández-García, Enhancing photocatalytic performance of TiO_2 in H_2 evolution via Ru co-catalyst deposition, *Appl. Catal., B*, 2018, **238**, 434–443.
48 J. M. Macak, B. G. Gong, M. Hueppe and P. Schmuki, Filling of TiO_2 nanotubes by self-doping and electrodeposition, *Adv. Mater.*, 2007, **19**, 3027–3031.
49 A. Gao, R. Hang, X. Huang, L. Zhao, X. Zhang, L. Wang, B. Tang, S. Ma and P. K. Chu, The effects of titania nanotubes with embedded silver oxide nanoparticles on bacteria and osteoblasts, *Biomaterials*, 2014, **35**, 4223–4235.
50 J. A. Seabold, K. Shankar, R. H. T. Wilke, M. Paulose, O. K. Varghese, C. A. Grimes and K. S. Choi, Photoelectrochemical properties of heterojunction CdTe/TiO_2 electrodes constructed using highly ordered TiO_2 nanotube arrays, *Chem. Mater.*, 2008, **20**, 5266–5273.
51 H. Yoo, K. Oh, G. Lee and J. Choi, RuO_2-Doped Anodic TiO_2 Nanotubes for Water Oxidation: Single-Step Anodization vs. Potential Shock Method, *J. Electrochem. Soc.*, 2017, **164**, H104–H111.
52 N. Denisov, J. E. Yoo and P. Schmuki, Effect of different hole scavengers on the photoelectrochemical properties and photocatalytic hydrogen evolution performance of pristine and Pt-decorated TiO_2 nanotubes, *Electrochim. Acta*, 2019, **319**, 61–71.
53 J. Huang, M. Hou, J. Wang, X. Teng, Y. Niu, M. Xu and Z. Chen, RuO_2 nanoparticles decorate belt-like anatase TiO_2 for highly efficient chlorine evolution, *Electrochim. Acta*, 2020, **339**, 1–9.
54 S. P. Hong, S. Kim, N. Kim, J. Yoon and C. Kim, A short review on electrochemically self-doped TiO_2 nanotube arrays: synthesis and applications, *Korean J. Chem. Eng.*, 2019, **36**, 1753–1766.
55 A. Ghicov, H. Tsuchiya, R. Hahn, J. M. MacAk, A. G. Muñoz and P. Schmuki, TiO_2 nanotubes: H^+ insertion and strong electrochromic effects, *Electrochem. Commun.*, 2006, **8**, 528–532.
56 H. Tokudome and M. Miyauchi, Electrochromism of titanate-based nanotubes, *Angew. Chem., Int. Ed.*, 2005, **44**, 1974–1977.
57 N. Sakai, A. Fujishima, T. Watanabe and K. Hashimoto, Highly Hydrophilic Surfaces of Cathodically Polarized Amorphous TiO_2 Electrodes, *J. Electrochem. Soc.*, 2001, **148**, E395.
58 A. R. Zeradjanin, T. Schilling, S. Seisel, M. Bron and W. Schuhmann, Visualization of chlorine evolution at dimensionally stable anodes by means of scanning electrochemical microscopy, *Anal. Chem.*, 2011, **83**, 7645–7650.
59 L. R. Bard and A. J. Faulkner, *Electrochemical Method: Fundamental and Applications*, John Wiley & Sons, Inc., New York, 2nd edn, 2001.